

## Early Stages of Gold and Silver Growth on $\alpha$ -MoTe<sub>2</sub>, $\beta$ -MoTe<sub>2</sub> and WTe<sub>2</sub>\*

Albert Prodan,<sup>a,\*\*</sup> Velibor Marinković,<sup>a</sup> Saw W. Hla,<sup>b</sup> Nina Ramšak,<sup>a</sup>  
Frank W. Boswell,<sup>c</sup> and J. Craig Bennett<sup>d</sup>

<sup>a</sup> *Institute Jožef Stefan, Ljubljana, Jamova 39, SI-1000 Slovenia*

<sup>b</sup> *Institut für Experimentalphysik, Freie Universität Berlin, Arnimalle 14,  
D-14195 Berlin, Germany*

<sup>c</sup> *Guelph-Waterloo Program for Graduate Work in Physics, Department of Physics,  
University of Waterloo, Waterloo, Ontario, Canada N2L 3G1*

<sup>d</sup> *Department of Physics, Acadia University, Wolfville, Nova Scotia,  
Canada B0P 1X0*

Received November 4, 1998; revised February 1, 1999; accepted February 2, 1999

The early stages of growth of gold and silver on (001) surfaces of  $\alpha$ -MoTe<sub>2</sub>,  $\beta$ -MoTe<sub>2</sub> and WTe<sub>2</sub> were studied by means of scanning tunneling microscopy. Metals were deposited at room temperature at a rate of about one monolayer per minute. It is shown that, prior to the epitaxial growth of the noble metal, a local interaction between the impinging atoms and the substrate takes place. During this period the noble-metal atoms diffuse through vacancies in the top tellurium layer and occupy enlarged interstices in the chalcogen–metal–chalcogen sandwich layers, where they agglomerate into one-atom-thick islands. Their shape and size depend on the stress between them and the substrate, and they remain stable at room temperature.

*Key words:* surface structure, surface reaction, scanning tunneling microscopy, noble metals, transition-metal dichalcogenides.

---

\* Dedicated to Professor Boris Kamenar on the occasion of his 70<sup>th</sup> birthday.

\*\* Author to whom correspondence should be addressed. (E-mail: albert.prodan@ijs.si)

## INTRODUCTION

With the accelerating trends towards increasing miniaturisation in modern technologies, a better insight into the nucleation and growth processes of metals on semiconducting surfaces is of crucial importance. The advent of the scanning tunneling microscope (STM)<sup>1</sup> and related instruments, like the atomic force microscope,<sup>2</sup> opened for the first time possibilities to investigate surface phenomena on an atomic scale and not only statistically. A precondition to control nucleation and growth processes at such a scale are *i.a.* substrate surfaces, whose structure is controlled on the same scale. Transition-metal dichalcogenides, and ditellurides ( $MTe_2$ ) in particular,<sup>3-7</sup> meet this requirement very well. First, their van der Waals (vdW) surfaces are chemically inert and clean substrates can be prepared by cleaving the crystals along the vdW gaps prior to introducing them into the ultra-high vacuum (UHV) system. Second, this family of compounds crystallises in a variety of related Te–M–Te sandwich structures with different periodically corrugated surfaces,<sup>8-10</sup> which strongly influence the way how the impinging metal atoms interact with the substrate.

Below about 1120 K  $MoTe_2$  crystallises in the  $\alpha$  form with the  $2H_b$ - $MoS_2$  structure (space group:  $P6_3/mmc$  (no. 194),  $a = 3.518 \text{ \AA}$ ,  $c = 13.974 \text{ \AA}$ ,  $Z = 2$ , Te in 4f and Mo in 2c positions).<sup>18,10</sup> The Te–Mo–Te sandwiches are built of  $MoTe_6$  trigonal prisms and are atomically flat perpendicular to the hexagonal  $c$ -direction (Figure 1). In contrast, in the high-temperature  $\beta$ - $MoTe_2$  form (space group:  $P2_1/m$  (no.11),  $a = 6.33 \text{ \AA}$ ,  $b = 3.469 \text{ \AA}$ ,  $c = 13.86 \text{ \AA}$ ,  $\beta = 93^\circ 55'$ ,

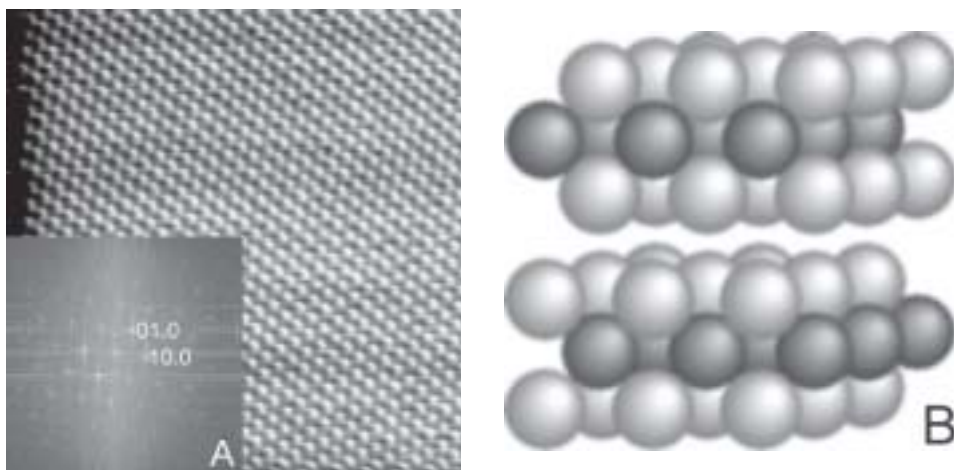


Figure 1. STM image of a defect free (001) surface of  $\alpha$ - $MoTe_2$  with the corresponding FFT (A) and a model of the structure (B) ( $100 \text{ \AA} \times 100 \text{ \AA}$ ,  $I_t = 3.5 \text{ nA}$ ,  $U_t = 5 \text{ mV}$ ,  $t = 300 \text{ \mu s}$ ).

$Z = 4$ , all atoms in 2e positions)<sup>8–10</sup> (Figure 2), these layers are periodically corrugated with the molybdenum atoms occupying deformed tellurium octahedra, which reduces the overall symmetry. The structure of WTe<sub>2</sub> (space group:  $Pmn2_1$  (no. 31),  $a = 6.270 \text{ \AA}$ ,  $b = 3.405 \text{ \AA}$ ,  $c = 14.028 \text{ \AA}$ ,  $Z = 4$ , all atoms in 4b positions)<sup>8–10</sup> is closely related to that of  $\beta$ -MoTe<sub>2</sub>, with the Te–W–Te sandwiches stacked in a slightly different way. Consequently, the two materials have similarly corrugated surfaces, which characteristically influence the growth of the metallic overlayer.

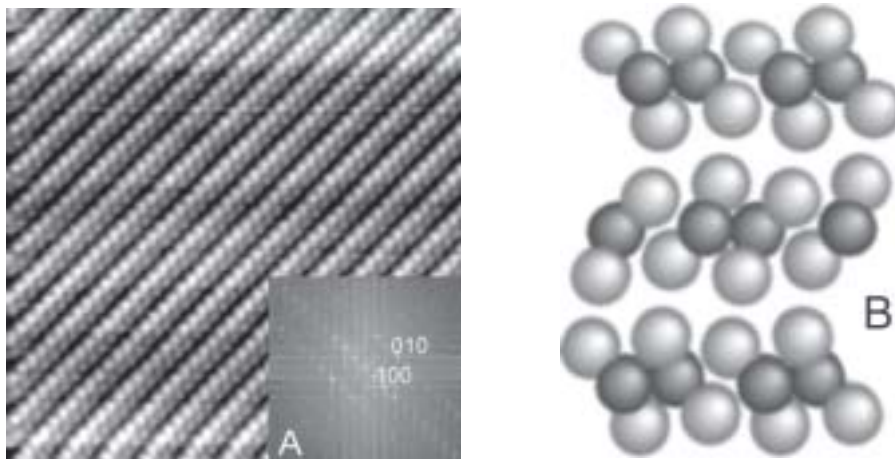


Figure 2. STM image of a defect free (001) surface of  $\beta$ -MoTe<sub>2</sub> with the corresponding FFT (A) and a model of the structure (B) ( $100 \text{ \AA} \times 100 \text{ \AA}$ ,  $I_t = 2.0 \text{ nA}$ ,  $U_t = 1 \text{ mV}$ ,  $t = 500 \text{ \mu s}$ ).

This paper describes a STM investigation of the behaviour of gold and silver during their earliest stages of growth on  $\alpha$ -MoTe<sub>2</sub>,  $\beta$ -MoTe<sub>2</sub>, and WTe<sub>2</sub> at room temperature. As it was shown earlier, copper and gold on WTe<sub>2</sub><sup>11</sup> as well as gold and silver on  $\alpha$ -MoTe<sub>2</sub> and  $\beta$ -MoTe<sub>2</sub><sup>12–14</sup> grow epitaxially at the ambient temperature, at which the surfaces of all three dichalcogenides used are stable and do not deteriorate with time under ultra-high vacuum conditions<sup>15</sup>.

## EXPERIMENTAL

The dichalcogenide single crystals were prepared by chemical transport reactions<sup>16</sup> with iodine as the transport agent. They were cleaved just before being introduced into the ultra-high vacuum chamber, where they remained clean and stable.

All experiments were carried out with an Omicron UHV-STM system, operated at a pressure between  $10^{-10}$  and  $10^{-11}$  mbar. Noble metals were evaporated from heated tungsten boats onto the dichalcogenide crystals kept at room temperature in an UHV sample preparation chamber, connected to the STM system. Deposition rates were approximately one monolayer per minute. Submonolayer thicknesses were controlled by adjusting the deposition times with a shutter after calibrating it on thicker deposits with a quartz balance. Prepared samples were transferred to the STM part without exposing them to ambient conditions.

All images described below were taken with the STM operated in the constant current mode (CCM), with typical pixel acquisition times between 300  $\mu$ s and 1000  $\mu$ s, and a fast Fourier transform (FFT) program was used for image filtering. Etched tungsten and cut platinum-rhodium (10%) tips were used throughout the work.

## RESULTS

In contrast to  $\alpha$ -MoTe<sub>2</sub>, in the case of  $\beta$ -MoTe<sub>2</sub> and WTe<sub>2</sub> the contribution of both sublattices to the STM images can be distinguished.<sup>3,7</sup> This is because the transition-metal and chalcogen sublattices are different. As shown in Figures 3 and 4, these contributions can vary greatly, depending on the tunneling conditions. Since this distinction allows a better insight into the processes during the earliest stages of growth, the results on  $\beta$ -MoTe<sub>2</sub> and WTe<sub>2</sub> substrates will be shown first.

### *The Growth on $\beta$ -MoTe<sub>2</sub> and WTe<sub>2</sub>*

The deformed MoTe<sub>6</sub> or WTe<sub>6</sub> octahedra, which form the sandwiches, give rise to a characteristic surface corrugation in the STM images. Although chalcogen layers only, without any contribution from the subsurface transition-metal layers, can be observed (Figure 2), more or less mixed contributions of both are commonly detected. Unfortunately, the contribution of both parts depends on the electronic states of the tip, which cannot be fully controlled by changing the tunneling conditions only. Instead, the images change abruptly during scanning as a result of an exchange of single tellurium atoms between the surface and the tip.

Although different in appearance, both Figure 3 and Figure 4 show  $\beta$ -MoTe<sub>2</sub> surfaces with a few deposited gold atoms. A careful analysis of Figure 3 reveals, in both parts of the image, different contributions of the two top-most atomic layers, while the top and bottom parts of Figure 4 show rather well separated molybdenum and tellurium contributions. The deposited gold atoms encounter pre-existing tellurium vacancies *via* surface diffusion, sinking through these into, presumably, the molybdenum layer and creating characteristic complex defects. These are visible in the upper part of Figure 3 and include one tellurium vacancy, slightly displaced from the

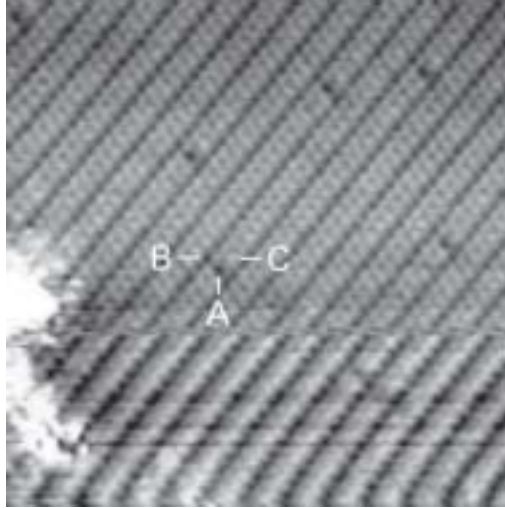


Figure 3. A typical (001) surface of  $\beta$ -MoTe<sub>2</sub> with a few identical defects, caused by thermally deposited gold ( $100 \text{ \AA} \times 100 \text{ \AA}$ ,  $I_t = 30 \text{ nA}$ ,  $U_t = 1 \text{ mV}$ ,  $t = 1000 \text{ \mu s}$ ). A, B and C represent a tellurium vacancy, a slightly enlarged tellurium–tellurium distance and a pushed up tellurium atom, respectively. A larger gold agglomerate is also visible in the lower left part of the image.

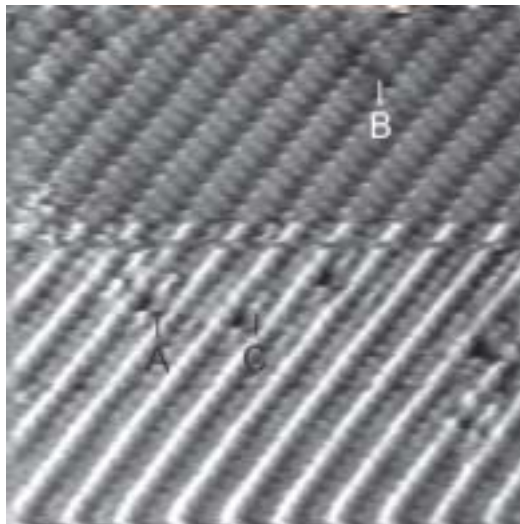


Figure 4. A (001) surface of  $\beta$ -MoTe<sub>2</sub> with the prevailing molybdenum (top) and tellurium (bottom) images ( $80 \text{ \AA} \times 80 \text{ \AA}$ ,  $I_t = 1.5 \text{ nA}$ ,  $U_t = 0.5 \text{ mV}$ ,  $t = 400 \text{ \mu s}$ ). A and B show the position of a gold atom in the two distinct images, while C refers to a tellurium atom pushed up from the lower tellurium chain.

lower tellurium chain (A), accompanied by visibly enlarged Te–Te distances along both adjacent tellurium chains (B) and by at least one elevated (*i.e.* brighter) neighbouring tellurium atom (C). Similar defects are observed in Figure 4, where the molybdenum and tellurium layers make the dominant tunneling contribution in, respectively, the top and bottom portions of the image, confirming these findings. The tellurium vacancies appear slightly displaced because of the gold atoms (A and B) occupying neighbouring enlarged interstices, which as a consequence elevate the two neighbouring tellurium atoms (C). It should be pointed out that the tellurium vacancies in most cases appear along the lower tellurium chains and only rarely along the top ones, since this is the easiest way to increase the interstitial volume. The described defects remain stable with time as well as during repeated scanning.

During further deposition, gold atoms continue to penetrate through the existing tellurium vacancies into the subsurface interstices and deform them, as shown in the case of gold deposited onto  $\text{WTe}_2$  (Figure 5). In the undeformed regions, the image shows only the top tellurium chains of the surface layer. Clearly visible are tellurium vacancies (A) accompanying the defect regions (B). In addition, however, rather blurred regions are also observed (C), which are attributed to some additional gold sitting on top of the tellurium surface. As a rule, these regions show no tellurium vacancies. It is

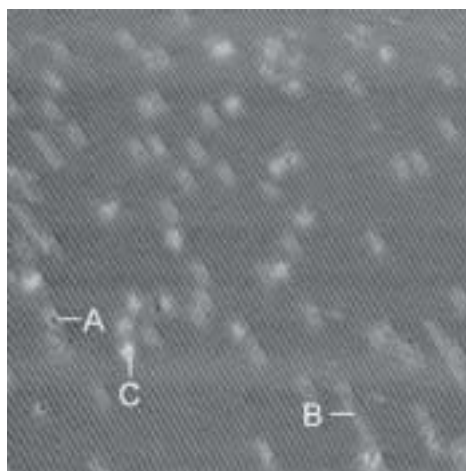


Figure 5. A tellurium surface layer of  $\text{WTe}_2$  during the initial stage of gold deposition ( $400 \text{ \AA} \times 400 \text{ \AA}$ ,  $I_t = 0.9 \text{ nA}$ ,  $U_t = 0.5 \text{ mV}$ ,  $t = 1000 \text{ \mu s}$ ). Gold atoms continue to diffuse through the existing tellurium vacancies (A), forming subsurface atomic chains (B). Some badly resolved regions with enhanced contrast (C) are believed to show additional gold sitting on the surface.

again useful to compare these findings with the corresponding ones for an image in which the tungsten atoms make the predominant contribution to the tunneling current (Figure 6). Again, two types of defect regions are distinguished. The first show deformations accompanying tellurium vacancies (A) with brighter intensity between two tungsten double chains, while the second (B) show only a smoothly enhanced contrast along the double tungsten chains. Both observations are in accord with the findings in Figure 5, with the second type of defect being caused by gold occupying a layer other than the two imaged ones.

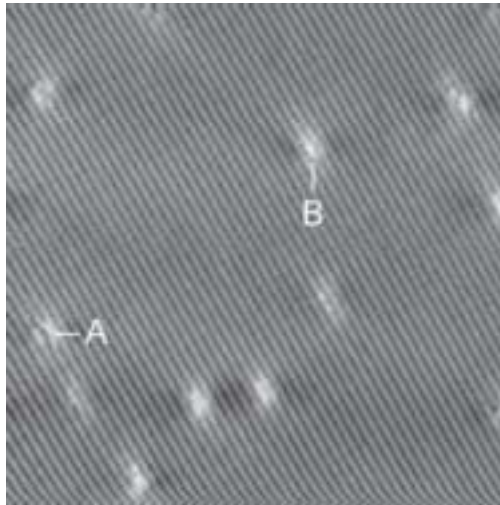


Figure 6. STM image of WTe<sub>2</sub> under tunneling conditions resolving the tungsten layer with two types of defect regions ( $300 \text{ \AA} \times 300 \text{ \AA}$ ,  $I_t = 0.9 \text{ nA}$ ,  $U_t = 0.5 \text{ mV}$ ,  $t = 1000 \text{ \mu s}$ ). The first show a deformed lattice with enhanced contrast between the double tungsten chains (A) and the second a smoothly enhanced contrast along otherwise undeformed tungsten chains (B).

With further deposition in-diffusion of gold is continued and the one-dimensional chains start to expand into two-dimensional strips, which finally cover the major part of the imaged area (Figure 7). Like the initial defects, these strips remain stable and do not change their appearance during repeated scanning. The image shows the distribution of the strips with numerous terminations (A). Because of the growing stress between the gold strips and the substrate, the first grow in width (*i.e.* perpendicular to the  $[1\bar{1}0]$  direction) only to about  $30 \text{ \AA}$ . This causes well defined lines perpendicular to the strips in the corresponding FFT (B).

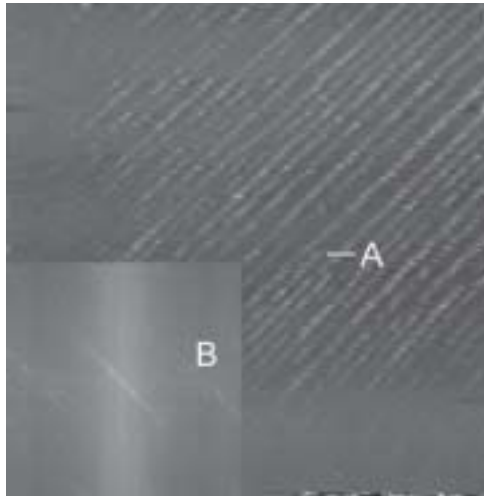


Figure 7. Two-dimensional strips of incorporated gold on  $\beta$ -MoTe<sub>2</sub> ( $2000 \text{ \AA} \times 2000 \text{ \AA}$ ,  $I_t = 1.0 \text{ nA}$ ,  $U_t = 1 \text{ mV}$ ,  $t = 1000 \text{ \mu s}$ ). Long strips with numerous terminations (A) give rise to well defined spikes in the corresponding FFT (B).

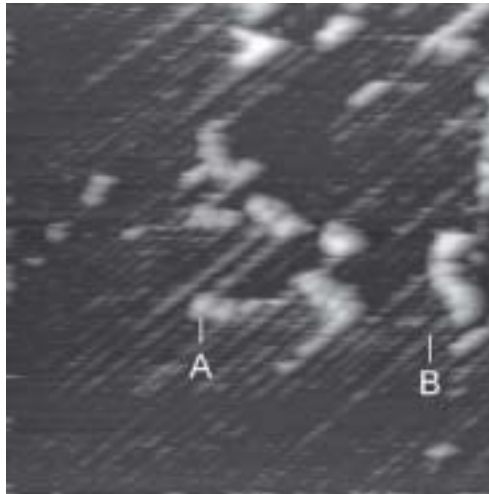


Figure 8. The growth of gold agglomerates (A) on the surface of  $\beta$ -MoTe<sub>2</sub> with strips of incorporated gold (B) ( $2000 \text{ \AA} \times 2000 \text{ \AA}$ ,  $I_t = 1.2 \text{ nA}$ ,  $U_t = 1 \text{ mV}$ ,  $t = 700 \text{ \mu s}$ ).

In thicker deposits, gold starts forming surface agglomerates of a few tens of atoms each (Figure 8). Contrary to the strips, these agglomerates are mobile and can easily be displaced by the strong local field of the scanning

tip. As a result, the agglomerates tend to join into islands, often elongated along the scanning direction, before they finally cover the surface as a continuous epitaxially grown film.<sup>12-15</sup>

The only difference between gold and silver is that silver often tends to form wider elongated islands, which is attributed to a greater mobility of silver as compared to that of gold.

### *The Growth on $\alpha$ -MoTe<sub>2</sub>*

The growth of gold and silver on  $\alpha$ -MoTe<sub>2</sub> is to some extent similar to that on the corrugated  $\beta$ -MoTe<sub>2</sub> and WTe<sub>2</sub>. However, in the case of  $\alpha$ -MoTe<sub>2</sub>, the two sublattices cannot be distinguished due to their similarity. The initial stage of gold growth on  $\alpha$ -MoTe<sub>2</sub> is shown in Figure 9. In analogy with

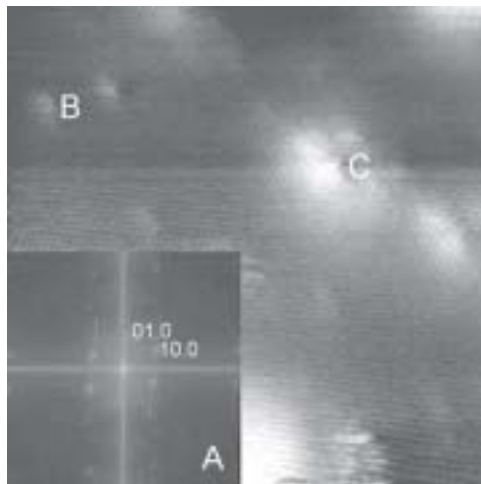


Figure 9. STM image of gold on  $\alpha$ -MoTe<sub>2</sub> with the corresponding FFT (A) ( $200 \text{ \AA} \times 200 \text{ \AA}$ ,  $I_t = 1.0 \text{ nA}$ ,  $U_t = 5 \text{ mV}$ ,  $t = 400 \text{ \mu s}$ ). Note the expanded areas of the surface tellurium layer (B) as well as gold atoms siting on top of these regions (C).

the observations on  $\beta$ -MoTe<sub>2</sub> and WTe<sub>2</sub>, these areas remain stable with time and are attributed to the expanded areas of the surface tellurium layer with gold occupying subsurface interstices. However, contrary to the previous case, no tellurium vacancies were observed in these regions. With additional gold deposited, the number of these expanded regions grows, until they uniformly cover the surface. The stress between the substrate and the defect regions allows these to grow in size only to a certain extent and prevents

their coalescence, again in analogy with the behaviour on the corrugated substrates.

Additional gold forms more or less round shaped agglomerates (A) on top of the surface (B) (Figure 10). The agglomerates are rather mobile and continue to grow until they reach an average size of a few tens of atoms each. Finally, the entire surface is covered by a thin epitaxially grown gold layer.<sup>12-15</sup>

Identical results were obtained with silver deposits.

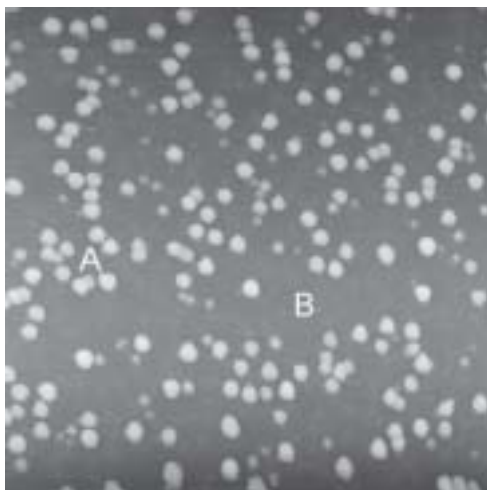


Figure 10. Gold agglomerates (A) and defect regions (B) on  $\alpha$ -MoTe<sub>2</sub> (2000 Å × 2000 Å,  $I_t = 0.25$  nA,  $U_t = 0.2$  V,  $t = 2000$  μs).

## DISCUSSION

The early stage of growth involves a diffusion of gold or silver atoms below the surface tellurium layer, *i.e.* into the tightly bonded Te–M–Te sandwich part of the structure. It should be noted that this kind of incorporation of noble metals was also observed in the case of single crystals of MoTe<sub>2</sub> grown from a mixture of MoTe<sub>2</sub> and gold or silver powders.<sup>16</sup> While the major part of the added noble metal (which did not exceed 2 atomic percent) formed separate (Au,Ag)Te<sub>2</sub> single crystals, known as the mineral Calaverite (space group:  $C2/m$  (no. 12),  $a = 7.1947$  Å,  $b = 4.4146$  Å,  $c = 5.0703$  Å,  $\beta = 90^\circ 2'$ ,  $Z = 2$ , Te in 4i and Au or Ag in 2a positions),<sup>19</sup> a small fraction was indeed found in both  $\alpha$ - and  $\beta$ -MoTe<sub>2</sub> crystals. After cleaving these crystals,

gold or silver was observed on the exposed surfaces (*i.e.* originally in the vdW gaps) mostly in the form of small agglomerates, but numerous defects, fully identical to those described in Figure 3 and Figure 4, were also detected. Thus, in addition to entering the vdW gaps, the noble metal atoms enter interstices in the Te–Mo–Te sandwiches as well.

It can be speculated about the reasons for the incorporation of the noble metal atoms into the tightly bonded Te–Mo(W)–Te sandwiches as well as about the positions they occupy. Regarding the latter, there are two possibilities. The noble metal atoms can, in principle, occupy the deformed tetrahedral, or by analogy with Calaverite, the octahedral interstices. The average structure of Calaverite may be considered as a squeezed CdI<sub>2</sub>-type structure with reduced vdW gaps (in the *c*-direction) and enlarged *a* and *b* unit cell constants. As a result, the metal atoms are in a deformed octahedral coordination with four long (2.98 Å) and two short (2.67 Å) Au(Ag)–Te distances, which change due to the structural modulation into two long and four short ones, dependent on whether gold is in the Au<sup>+</sup> or Au<sup>3+</sup> state. On the other hand, the deformed octahedra in the structures of  $\beta$ -MoTe<sub>2</sub> and WTe<sub>2</sub> have three long (about 2.8 Å) and three short (about 2.7 Å) Mo(W)–Te distances.<sup>10</sup> Since both gold and silver behave in the same way and since silver can be in the Ag<sup>+</sup> state only, it is believed that the coordination with four long and two short Au(Ag)–Te distances will be preferred. By pushing out the originally lower lying tellurium atoms (about 0.4 Å) at both sides of the Te–Mo(W)–Te sandwiches, an almost ideal coordination for the interstitial gold or silver atoms can be obtained. In this case, however, the molybdenum lattice must be deformed to make room for the interstitial noble metal atom. Due to the mixed character of the bonding, the local charge can easily be balanced by the surrounding molybdenum or tungsten ions.

*Acknowledgement.* – Thanks are due to Mrs. Zora Škraba for preparing the single crystals. The authors also thankfully acknowledge a financial support of the Ministry of Science and Technology of the Republic of Slovenia (AP, SWH) and of the Natural Science and Engineering Research Council of Canada (FWB, JCB). A NATO Expert Visit Grant (AP) was helpful in facilitating the collaboration.

## REFERENCES

1. G. Binnig, H. Rohrer, C. Gerber, and E. Weibel, *Phys. Rev. Lett.* **50** (1983) 120–123.
2. G. Binnig, C. F. Quate, and C. Gerber, *Phys. Rev. Lett.* **56** (1986) 930–933.
3. S. L. Tang, R. V. Kasowski, and B. A. Parkinson, *Phys. Rev. B* **39** (1989) 9987–9991.
4. S. L. Tang, R. V. Kasowski, A. Suna, and B. A. Parkinson, *Surf. Sci.* **238** (1990) 280–288.
5. A. Crossley, S. Myhra, and C. J. Sofield, *Surf. Sci.* **318** (1994) 39–45.
6. J. A. A. Crossley, C. J. Sofield, and S. Myhra, *Surf. Sci.* **380** (1997) 568–575.
7. S. W. Hla, V. Marinković, A. Prodan and I. Mušević, *Surf. Sci.* **352–354** (1996) 105–111.
8. B. E. Brown, *Acta Crystallogr.* **20** (1966) 268–274.
9. W. G. Dawson and D. W. Bullett, *J. Phys. C: Solid State Phys.* **20** (1987) 6159–6174.
10. F. Hulliger, *Transition-Element Compounds with Octahedral Cation Coordination*, in: F. Lévy (Ed.), *Structural Chemistry of Layer-Type Phases, Physics and Chemistry of Materials with Layered Structures*, Vol. 5, D. Reidel, Dordrecht, 1976, pp. 210–242.
11. M. L. Bortz, F. S. Ohuchi, and B. A. Parkinson, *Surf. Sci.* **223** (1989) 285–298.
12. S. W. Hla, V. Marinković, and A. Prodan, *Vuoto* **25** (1996) 84–86.
13. S. W. Hla, V. Marinković, and A. Prodan, *Surf. Sci.* **356** (1996) 130–136.
14. S. W. Hla, V. Marinković, and A. Prodan, *Surf. Sci.* **377–379** (1997) 979–982.
15. S. W. Hla, V. Marinković, and A. Prodan, *Thin Solid Films* **317** (1998) 14–16.
16. H. Schöfer, *Chemical Transport Reactions*, Academic Press, New York, 1964.
17. Unpublished data.
18. O. Knop and R. D. MacDonald, *Can. J. Chem.* **39** (1961) 897–904.
19. W. J. Shute and J. L. de Boer, *Acta Crystallogr., Sect. B* **44** (1988) 486–494.

## SAŽETAK

Početne faze rasta zlata i srebra na  $\alpha$ -MoTe<sub>2</sub>,  $\beta$ -MoTe<sub>2</sub> i WTe<sub>2</sub>

*Albert Prodan, Velibor Marinković, Saw W. Hla, Nina Ramšak,  
Frank W. Boswell i J. Craig Bennett*

Početna faza rasta naparenog zlata i srebra na (001) površinama  $\alpha$ -MoTe<sub>2</sub>,  $\beta$ -MoTe<sub>2</sub> i WTe<sub>2</sub> proučavana je s pomoću tunelske mikroskopije. Metali su naparavani brzinom oko jednog monoatomnog sloja u minuti, dok je substrat održavan na sobnoj temperaturi. U toj fazi dolazi do interakcije između upadnih atoma i substrata, pri čemu metalni atomi difundiraju kroz praznine u površinskom sloju telurija te zaposjedaju i povećaju intersticije u strukturi halkogen–metal–halkogen. Ti su aglomerati stabilni na sobnoj temperaturi, a njihova veličina i oblik ovise o napetosti između njih i podloge.